Simulating the collapse of unsaturated soil by DEM

S. H. Liu[1,*,†] and D. A. Sun[2]

[1] *East China Investigation & Design Institute, Shangtang Road, Hangzhou, 310014, People's Republic of China*
[2] *VBL, Nagoya Institute of Technology, Gokiso-cho, Showa-ku, Nagoya, 466-8555, Japan*

SUMMARY

This paper presents a numerical method to simulate the collapse behaviours of unsaturated soils by distinct element method (DEM). The influence of suction in unsaturated soil is reproduced in DEM simulation by introducing an interparticle adhesive force that acts perpendicular to the tangential plane at contact point. A biaxial compression test on an assembly of circular rigid particles is numerically simulated using DEM by incorporating interparticle adhesive forces. The collapse behaviours of unsaturated soils during isotropic compression and biaxial shear are simulated by means of releasing the interparticle adhesive forces from the initially incorporated values to zero at constant stress state. The numerically simulated results are then compared with the results of triaxial compression tests on unsaturated compacted clays and qualitative similarities are obtained. The influences of the mean stress, the stress ratio and the interparticle adhesive force on the collapse behaviours are numerically investigated. The fabric structure and the particle stability of the simulated specimen before and after collapse are also investigated and discussed. Copyright © 2002 John Wiley & Sons, Ltd.

KEY WORDS: collapse; distinct element method; interparticle adhesive force; unsaturated soil

1. INTRODUCTION

Volume decreases accompanying increases in water content at essentially unchanging total stresses in loose, partly saturated natural soil deposits have been termed collapse. Collapse can occur in many naturally deposited soils, especially aeolian deposits of loess and sand, at low stress levels [1] and in compacted soils at high stress levels. Considerable experimental researches have been conducted to study collapse of naturally deposited or artificially compacted soils [2–7] using both a conventional or double oedometre and a triaxial laboratory test, and several soil models [8–11] have been proposed for modelling the collapsing soil behaviour.

Four factors are necessary for collapse to occur in soil [12,13]:

- An open, partially unstable, partially saturated fabric.
- A high enough total stress that the structure is metastable.
- A bonding or cementing agent that stabilizes the soil in the partially saturated condition.

————————
*Correspondence to: Sihong Liu, Nakata-so 7-503, Wakamizu 2-4-7, Chikusa-ku, Nagoya 464-0071, Japan
†E-mail: sihong@doboku2.ace.nitech.ac.jp

● The addition of water to the soil, which causes the bonding or cementing agent to be reduced and the interaggregate or interparticle contacts to fail in shear, resulting in a reduction in total volume of the soil mass.

For unsaturated granular material, the metastable bonding is typically provided by capillary suction. A relationship can be established between such capillary suction and interparticle adhesive force that acts perpendicular to the contact plane of soil particles. It is possible to study numerically the deformation and strength characteristics of unsaturated soil using discrete element method [14] by incorporating interparticle adhesive force [15]. If the interparticle adhesive force is released under a constant stress state that approximately simulates the addition of water to a collapsible soil, then it is also possible to study numerically the collapse behaviour of unsaturated granular material by means of DEM. In this paper, we introduce this numerical method and present the simulation results for a biaxial compression test on a two-dimensional model granular material. The calculated results are compared with some experimental results on unsaturated compacted clays. Qualitative similarities for the collapse behaviours are obtained between calculated and experimental results. Moreover, some microscopic studies on the fabric and particle stability of the simulated specimen are also investigated and discussed.

2. SUCTION AND INTERPARTICLE ADHESIVE FORCE

It is well-known that both air and water exist inside a void of an unsaturated soil. Figure 1 shows an enlarged picture of water attachment in an assembly of wet cylindrical aluminium rods [16,17]. It is seen from Figure 1 that some water is absorbed surrounding the contact of particles due to the capillary action. This capillary water creates a meniscus on its surface and then generates a suction s and an interparticle force P_s due to the surface tension T of the capillary
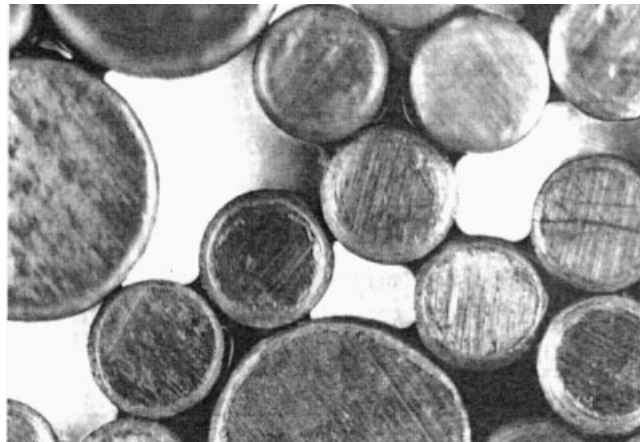

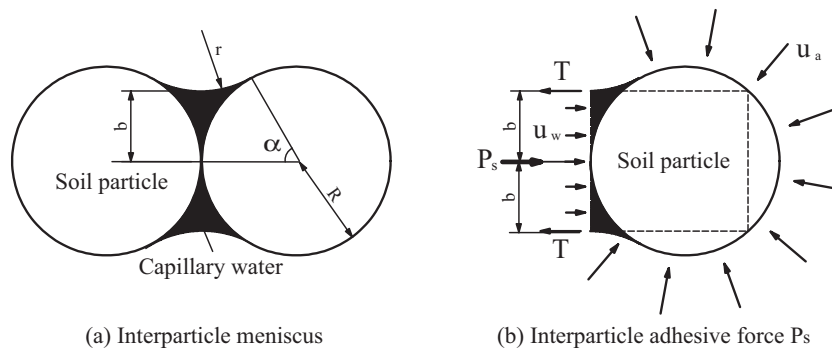Figure 1. Enlarged picture of water attachment in an assembly of wet circular aluminium rods (after [16,17]).

Figure 2. Interparticle adhesive force due to water meniscus.

water, which can be calculated by the following equations (cf. Figure 2):

$$\left.\begin{array}{l} s = u_a - u_w = T/r \\ P_s = (u_a - u_w)2b + 2T \end{array}\right\} \quad \text{(for cylindrical aluminium rods)} \tag{1}$$

$$\left.\begin{array}{l} s = u_a - u_w = T(1/r - 1/b) \\ P_s = (u_a - u_w)\pi b^2 + T(2\pi b) \end{array}\right\} \quad \text{(for spherical soil particles)} \tag{1'}$$

where r and b are the radii of meniscus and capillary water cylinder at its centre, respectively. They can be expressed with the radius R of particle and the angle α of capillary water retention from the geometrical consideration by Equations (2) and (3).

$$b = R(\tan \alpha + 1 - \sec \alpha) \tag{2}$$

$$r = R(\sec \alpha - 1) \tag{3}$$

The real soil particle may not be cylindrical or spherical as shown in Figure 2, but meniscus and its capillary action usually exist in a partially saturated soil when the degree of saturation is low, which induce an interparticle adhesive force. This interparticle adhesive force affects the mechanical behaviours of partially saturated soil. In this paper, we try to simulate the collapse phenomenon of an unsaturated granular material using DEM by incorporating an interparticle adhesive force at particle contacts and then releasing it under a constant stress state.

By the way, the interparticle force P_s induces an internal bonding stress σ_s in the specimen that can be estimated by Equation (4) [18].

$$\sigma_s = \frac{2P_s}{\pi^2 R_m^2 (1 + e)} \tag{4}$$

where R_m is the average radius of the particles along mobilized plane and e is the void ratio of the specimen. This internal bonding stress σ_s is considered to be equivalent to the suction stress $\sigma_0(s)$ that is defined for unsaturated soils and has a hyperbolic relationship with suction s [11]. For a given sample, the interparticle force P_s has thereby a hyperbolic relationship with suction s, too.

3. BIAXIAL COMPRESSION SIMULATION

3.1. Outline of DEM analysis incorporated with an interparticle adhesive force

Only a brief introduction to two-dimensional distinct element method (DEM) is given here. DEM is a numerical technique where individual particles are represented as rigid bodies. In two dimensions each particle has three degrees of freedom (two translations and one rotation). Each particle can be in contact with neighbouring particles or structure boundaries. The contact between two particles, or a particle and a boundary, is modelled with a spring and dashpot in both the normal and tangential directions. The normal direction spring has a no-tension constraint. In the tangential direction, if the tangential force reaches a Coulomb friction limit, it is allowed to slide. Small amounts of viscous damping are often included to help provide dissipation of high-frequency motion. The forces generated at a contact are computed based on the overlap of the bodies at the contact and the stiffness of the springs.

In this study, the computer code of DEM is GRADIA that was programmed by Yamamoto [19]. In order to account for the effect of suction existing in unsaturated soil, we incorporate an interparticle adhesive force at contacts in GRADIA. If the interparticle adhesive force that acts perpendicular to the contact plane between particles i and j is denoted as P_{sij}, then the components of the resultant forces in x and y directions as well as the resultant moment acting on particle i due to P_{sij} are given by the following equations:

$$[F_{xi}^{\mathrm{p}}]_t = \sum_j P_{sij} \cos \alpha_{ij}$$

$$[F_{yi}^{\mathrm{p}}]_t = \sum_j P_{sij} \sin \alpha_{ij} \qquad (5)$$

$$[M_i^{\mathrm{p}}]_t = 0$$

where α_{ij} is the inclined angle of the line connecting the centres of contacting particles i and j to the x-axis. The force components due to the interparticle adhesive force P_{sij} calculated from Equation (5) are thereafter added into the forces based on the overlap of the bodies at the contact and the stiffness of the springs yielding a final resultant force, which is then used to compute the acceleration of the body according to Newton's law of motion. After the acceleration is determined, new velocity and displacement for the particle is computed using central difference explicit time integration. With the newly computed displacement configuration, the state of deformation at existing contacts is re-evaluated, and the possible creation of new contacts is evaluated, leading to a new cycle of computation.

3.2. Biaxial compression simulation

Initially, a DEM specimen of 5443 circular particles is generated randomly within a 60 cm × 30 cm rectangular area that is bounded by four rigid walls. The particles have two different sizes with diameters of 5 and 9 mm and a mixing ratio of 3:2 by area. The specimen has an initial void ratio of 0.262. The input parameters used in our DEM simulation are summarized in Table I. Yamamoto [19] used the same parameters to simulate a biaxial compression test on an assembly of aluminium rods with diameters of 5 and 9 mm and a mixing ratio of 3:2 by weight. His calculation results agreed very well with the experimental results.

Table I. Input parameters for numerical simulation by DEM.

	Particle–Particle	Particle–platen
Normal stiffness k_N, k'_N (N/m/m)	9.0×10^9	1.8×10^{10}
Shear stiffness k_S, k'_S (N/m/m)	3.0×10^8	6.0×10^8
Normal damping η_N, η'_N (N s/m/m)	7.9×10^4	1.1×10^5
Shear damping η_S, η'_S (N s/m/m)	1.4×10^4	2.0×10^4
Interparticle friction angle ϕ_μ, ϕ'_μ (deg)	16	16
Density of particle ρ (kg/m^3)	2700	
Time increment Δt (s)	2×10^{-7}	

As the surface tension of water, T, is a constant (about 0.0745 N/m when water temperature is 20°C), it is seen from Equations (1)–(3) that for 2D cylindrical rods, the interparticle adhesive force P_s is independent of the radii R of the cylindrical aluminium rods if the angle α of capillary water retention is assumed constant (in fact, α ranges from 15 to 20° for the cylindrical aluminium rods according to the experimental measurements [16]). Thus, in our simulation, a constant value of P_s is applied at each contact point irrespective of what radii of two contacting circular particles. This simple hypothesis is suitable for 2D cylindrical rods and might not exactly model a real unsaturated soil. For a real unsaturated soil, the value of P_s differs from the size and shape of soil particles, the pore water states inside soil voids and so on. It needs further study and development of the exact simulation for the real unsaturated soil.

In this study, the predetermined interparticle adhesive forces are introduced to the contacts between particles at initial specimen. Each specimen is isotropically compressed under increasingly mean stress $p = (\sigma_1 + \sigma_3)/2$ ($\sigma_2 = 0$ for biaxial compression). At some previously specified mean stresses, the incorporated interparticle adhesive force is released gradually to zero to simulate the collapse phenomenon of unsaturated soil during compression. Then, the specimen is sheared at a constant confining pressure $\sigma_3 = 98$ kPa as well as at a constant mean stress $p = 196$ kPa. Under each stress state, the interparticle adhesive force incorporated in the specimen is released gradually to zero at different constant principal stress ratios to simulate the collapse phenomenon of unsaturated soil during shear.

4. EXPERIMENTAL AND SIMULATED RESULTS

4.1. Experimental results on unsaturated compacted Kaolin-clay

First, we present some experimental results of triaxial compression tests on unsaturated compacted Kaolin-clay [11,20], which will be used to compare qualitatively with the results of the numerically simulated biaxial compression test. The laboratory tests were conducted in an improved triaxial cell for controlling suction by adopting the axis translation technique and measuring directly the lateral strain of specimens with two bronze-made rings. The Kaolin-clay specimen had a dry density of about 1.15 g/cm^3, a void ratio of about 1.35, and a degree of saturation of about 50%. Figure 3 shows the volume change of the unsaturated compacted Kaolin-clay during isotropic compression [20]. The identically compacted specimens were isotropically compressed under constant matric suction of 147 kPa and then allowed to consolidate at various steps of decreasing matric suction from 147 to 0 kPa under a previously
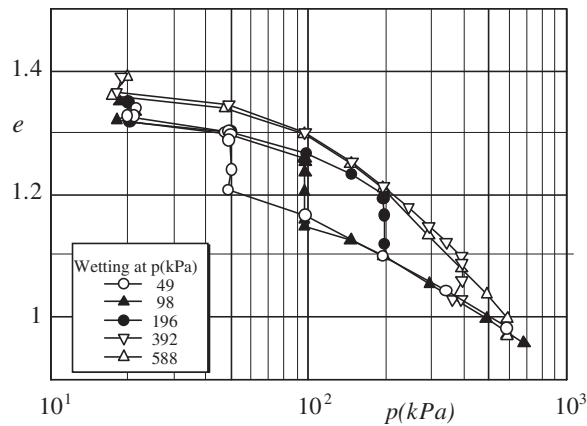
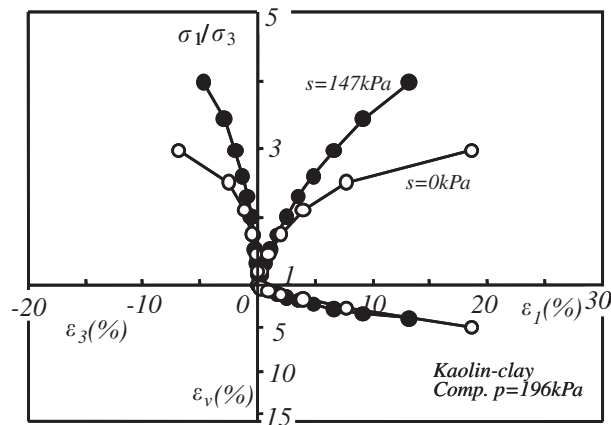Figure 3. Volume change of compacted Kaolin-clay under isotropic compression with wetting (after [20]).

Figure 4. Results of triaxial compression tests on saturated and unsaturated compacted Kaolin-clay at constant mean net pressure $p = 196$ kPa (after [11]).

specified net confining pressure. It can be seen from Figure 3 that the magnitude of volume change (collapse) due to the reduction of matric suction depends on the applied mean net stress and the compression curves after collapse are closely arranged on a unique curve. Figure 4 compares the stress–strain relationships of the saturated ($s = 0$ kPa) and unsaturated ($s = 147$ kPa) compacted Kaolin-clay that are sheared at constant mean stress $p = 196$ kPa. It illustrates that the shear strength of the soil increases with an increasing suction. Figure 5 shows the stress–strain relationships of the unsaturated compacted Kaolin-clay during shear under constant mean stress $p = 196$ kPa accompanying with matric suction s decreased from 147 to 0 kPa (causing collapse) at different stress ratios. It can be seen from Figure 5 that the magnitude of vertical collapsing strain ε_1 increases (compression) and the magnitude of lateral collapsing strains ε_3 decreases (extension) with an increasing stress ratio. However, the
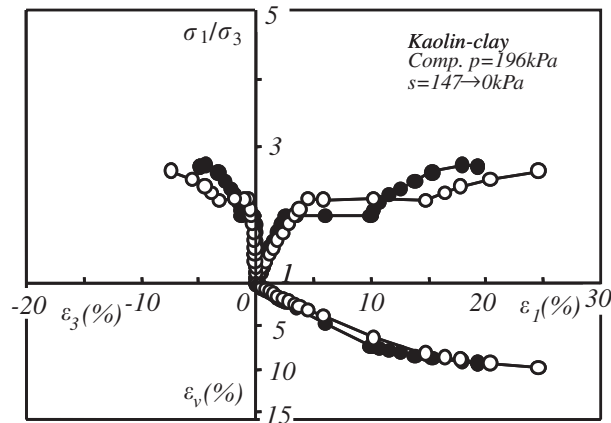
Figure 5. Collapse behavior of compacted Kaolin-clay at different stress ratios obtained from triaxial compression tests (after [11]).
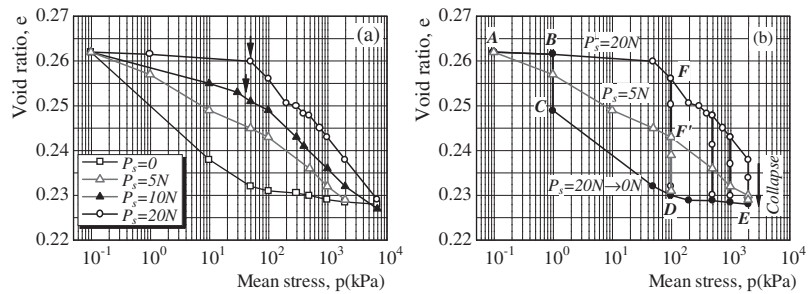

Figure 6. Volume changes of numerically simulated biaxial compression tests during isotropic compression.

magnitudes of volumetric collapsing strain ε_v are almost the same when the matric section is reduced at different stress ratios.

4.2. Volume changes under isotropic compression stress obtained from DEM simulation

Figure 6 shows the volume changes of the numerically simulated biaxial compression specimens with respect to the applied mean stress (i.e. compression curve). The interparticle adhesive forces P_s of 0, 5, 10 and 20 N are, respectively, incorporated into the initial specimens, which are, respectively, equivalent to the internal bonding stresses σ_s of 0, 65, 130 and 260 kPa estimated by Equation (4). Figure 6(a) illustrates the influences of the incorporated interparticle adhesive force P_s on the volume changes. It is seen from Figure 6(a) that the $e \sim \ln p$ curves for the specimens with and without interparticle adhesive force P_s converge at high mean stresses where no collapse occurs when P_s is completely decreased and there may exist a yield stress for the specimen with a specified interparticle adhesive force P_s. This yield stress appears clearly and increases with increasing P_s. The little volume reduction of the specimen with $P_s = 0$ N when the mean stress p exceeds to 100 kPa in Figure 6(a) may be caused by the assumption of rigid

particles in our DEM simulation so as to no particle crushing takes place even under high compression pressure as usual soils. Figure 6(b) illustrates the collapse deformations induced by releasing the interparticle adhesive force P_s from the initially incorporated value to zero at different mean stresses that approximately simulate the inundation to an unsaturated soil. The compression curve BCDE in Figure 6(b) is obtained by compressing the specimen to $p = 2000$ kPa after P_s is reduced from 20 to 0 N at $p = 1$ kPa, which is almost identical with the compression curve corresponding to the specimen with initial $P_s = 0$ N as shown in Figure 6(a). It is seen from Figure 6(b) that the collapse deformation induced by releasing the interparticle adhesive force depends on the applied mean stress p and the initially incorporated interparticle adhesive force P_s. Its magnitude increases with increasing interparticle adhesive force P_s at the same mean stress p; for example, at the same mean stress p of 98 kPa, the collapse deformation of the specimen with $P_s = 20$ N (denoted by FD) is larger than that for the specimen with $P_s = 5$ N (denoted by F'D). However, the specimens have almost the same void ratios as in the saturated state ($P_s = 0$ N) after collapse occurs either for $P_s = 20$ N or for $P_s = 5$ N. It is also found that for the specimen with a specified interparticle adhesive force P_s, the collapse deformation increases with the increases in the applied mean stress when the applied mean stress is less than the yield stress and decreases with the increases in the applied mean stress when the applied mean stress exceeds the yield stress. Yudhbir [21] reported the similar collapse characteristics observed from the experiments on unsaturated soils and Sun *et al.* [11] proposed an elasto-plastic model to predict such characteristics. Moreover, the DEM simulation results shown in Figure 6 are quite similar to the results of triaxial compression tests on unsaturated compacted Kaolin-clay as shown in Figure 3, thus illustrating the reasonability of the numerically simulated results.

Figure 7 shows the volume change progressed with the release of the interparticle adhesive force P_s at different mean stresses for the specimens with an initial $P_s = 20$ N. It can be seen that the rate of volume change induced by releasing P_s from 20 to 10 N is less than that induced by releasing P_s from 10 to 0 N. Pereira *et al.* [7] also reported the phenomenon that the rate of volume change is less in high suction than that in low suction based on the experimental results for a compacted residual gneiss soil. They suggested that at high suction, the soil undergoes
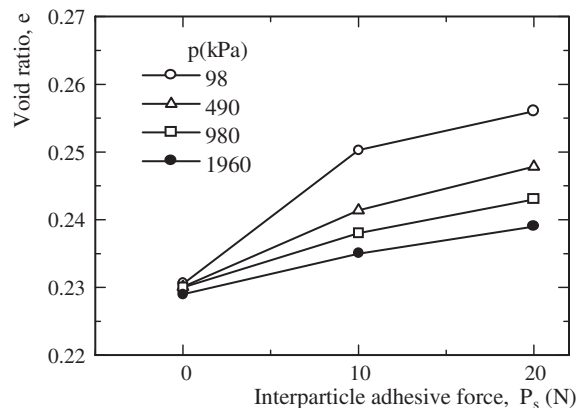

Figure 7. Collapse process at different mean stress for the specimen with an initial $P_s = 20$ N.

elastic compression without grain slippage resulting in small compressibility due to a change in matric suction, and at relatively high suction, the soil suffers significant volumetric deformations caused by both the soil structural rearrangements and the occurrence of local shearing of grains in response to the suction reduction. Kohgo *et al.* [22] interpreted this phenomenon as an internal confinement for soil particles by interparticle adhesive force P_s resulting from capillary force. This internal confinement becomes stronger at higher suction due to the expansion of unsaturated area. The above suggestions can also explain the phenomenon shown in Figure 7. Moreover, Figure 7 suggests that collapse deformation is a plastic deformation and affected by both suction and applied external stress.

4.3. Collapse behaviours under shear stress obtained from DEM simulations

Figures 8(a) and 8(b) show the stress–strain relationships of the numerically simulated biaxial compression tests on the samples with inpterparticle adhesive forces $P_s = 0$ and 5 N during shear under constant mean stress $p = 196$ kPa and constant confining stress $\sigma_3 = 98$ kPa, respectively. It can be seen from Figure 8 that the stress ratio for the specimen with $P_s = 5$ N is larger than that for the specimen with $P_s = 0$ N at the same strains at each stress state, which is similar to the experimental results for the unsaturated and saturated compacted Kaolin-clay as shown in Figure 4. Thus, it is understood that the interparticle adhesive force P_s has the same contributions to the stress–strain relations as matric suction in unsaturated soils.

Figures 9(a) and 9(b) show the results of the numerically simulated biaxial compression tests during shear under constant mean stress $p = 196$ kPa and constant confining stress $\sigma_3 = 98$ kPa with the interparticle adhesive force P_s released from 5 to 0 N at different principal stress ratios, respectively. It can be seen from them that, irrespective of the stress paths of $p = 196$ kPa and $\sigma_3 = 98$ kPa, the magnitude of vertical collapsing strain ε_1 increases (compression) and the magnitude of lateral collapsing strains ε_3 decreases (extension) with an increasing principal stress ratio. However, the magnitude of volumetric collapsing strain ε_v depends weakly on the principal stress ratio. These behaviours are similar to the experimental results on unsaturated soils as shown in Figure 5 or as observed by Lawton *et al.* [5]. It can also be seen from Figure 9 that the stress–strain responses tend to be the same and coincide nearly with those in the case of $P_s = 0$ after collapse takes place at different stress ratios.
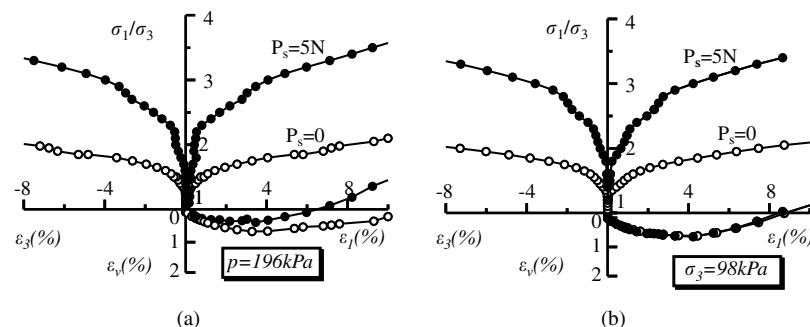

Figure 8. Stress–strain relationships of numerically simulated biaxial compression tests on samples with interparticle adhesive force $P_s = 0$ N and 5 N: (a) at constant mean stress $p = 196$ kPa and (b) at $\sigma_3 = 98$ kPa.
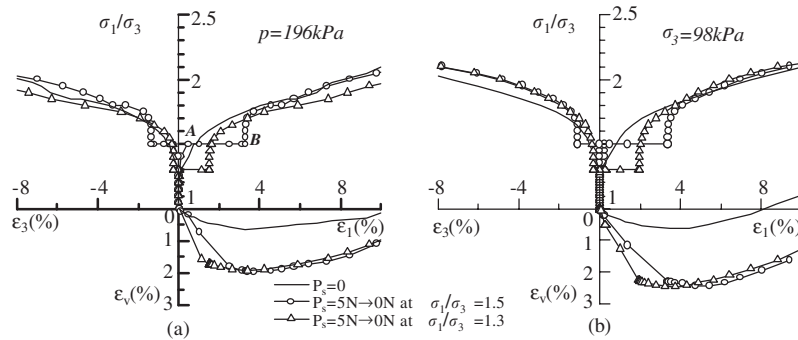
Figure 9. Collapse behaviours of numerically simulated biaxial compression tests during shear at different stress ratios: (a) under constant mean stress $p = 196$ kPa; and (b) under constant confining stress $\sigma_3 = 98$ kPa.
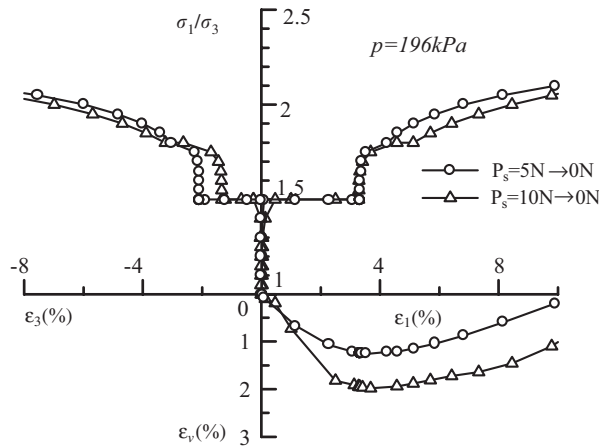

Figure 10. Influence of interparticle adhesive force P_s on collapse behaviour during shear obtained from DEM simulation.

Figure 10 shows the influence of the interparticle adhesive force P_s on the collapsing behaviour under shear. It illustrates that the magnitude of volumetric collapsing strain ε_v induced by releasing P_s from 10 to 0 N is larger than that induced by releasing P_s from 5 to 0 N. This may suggest that the magnitude of the volume change increases with an increasing suction in unsaturated soils.

5. MICROSCOPIC INVESTIGATIONS ALONG WITH COLLAPSE

The fabric structure of the specimen and the stability between the contacting particles may be changed accompanying with collapse. The fabric structure can be characterized by a polar histogram distribution of contact normals $M(\theta)$ defining the total numbers of contacts corresponding to contact angle θ. To illustrate the stability between the contacting particles, we

introduce index ρ as the ratio of shear force to the Coulomb friction strength at a contact, expressed as

$$\rho = \frac{|f_s|}{f_n \tan \phi_\mu} \tag{6}$$

where f_s and f_n are the shear and normal force at the contact, respectively; and ϕ_μ the interparticle friction angle. When the contact shear force equals the Coulomb friction strength, the index ρ takes the value of 1.0 where slip between the particles occurs. The smaller value of the index ρ is, the more stable the contacting particles will be. For unsaturated soils, the shear and normal contact forces, f_s and f_n, at any typical contact point are caused by both external and the interparticle adhesive forces that are expressed as

$$f_s = T$$
$$f_n = N + P_s \tag{7}$$

where N and T are, respectively, the normal and shear forces caused by external forces. The maximum possible shear resistance T_{max} at grain contact points will be

$$T_{max} = f_n \tan \phi_\mu = N \tan \phi_\mu + c_s$$
$$c_s = P_s \tan \phi_\mu \tag{8}$$

where c_s denotes the contribution of the interparticle adhesive force P_s to the shear resistance. In most of the problems usually encountered in the field, c_s is independent of the external forces, since pore air is always connected with the atmosphere with the pressure almost equal to the atmospheric pressure and pore water pressure is not affected by the external forces in a low saturation. Thus, c_s may be regarded as a nominal cohesion [22].

Figures 11(a) and 11(b) show the polar histogram distributions of contact normals and the index ρ when releasing the interparticle adhesive force P_s from 20 to 0 N at isotropic compression stress $p = 100$ kPa corresponding to the points $F \rightarrow D$ in Figure 6(b), respectively. It can be seen from Figure 11(a) that the number of contacts at any orientation increases after
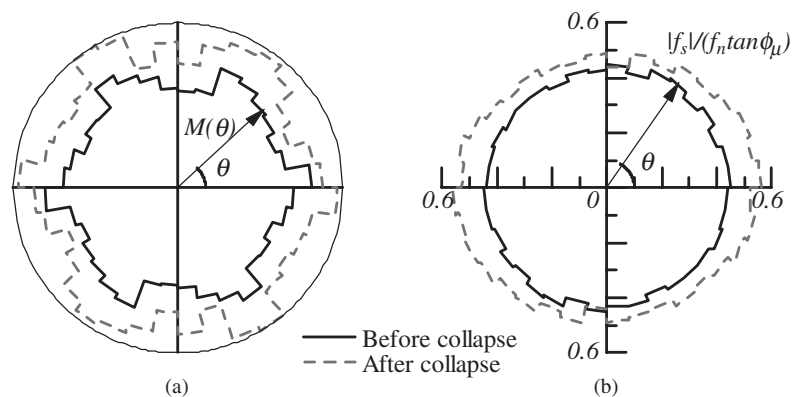

Figure 11. Variation of contact normals and contact force ratios when interparticle adhesive force P_s released from 20 to 0 N at isotropic compression pressure $p = 100$ kPa ($F \rightarrow D$ in Figure 6(b)): (a) contact normals; (b) contact force ratios.
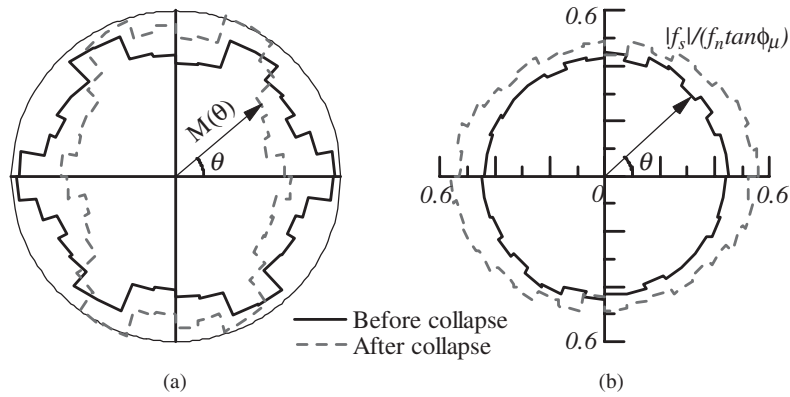
Figure 12. Variation of contact normals and contact force ratios during shearing at constant $p = 196$ kPa with interparticle adhesive force P_s released from 5 to 0 N at the stress ratio = 1.5 ($A \rightarrow B$ in Figure 9(a)): (a) contact normals; (b) contact force ratios.
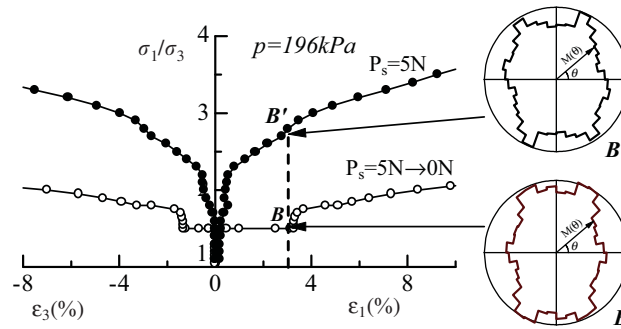

Figure 13. Distributions of contact normals for the specimen with P_s deduced from 5 to 0 N and for the specimen with $P_s = 5$ N at the same shear strains.

the incorporated P_s between particles is released at constant compression mean stress, which coincide qualitatively with the characteristics of soils observed during isotropic compression. After releasing P_s (collapse), the index ρ increases at any orientation as shown in Figure 11(b), which means the decrease of the stability of the contacting particles. This phenomenon can be explained from formula (8). Before collapse, there is a contribution c_s of the interparticle adhesive force P_s to the shear resistance that inhibits the relative sliding between the particles. After collapse, this contribution vanishes, resulting in the decrease of the stability of the contacting particles.

Figures 12(a) and 12(b) show the polar histogram distributions of contact normals and the index ρ before and after releasing P_s from 5 to 0 N at constant stress ratio (causing collapse during shear) corresponding to the points $A \rightarrow B$ in Figure 9(a), respectively. It can be seen that the distribution of contact normals becomes more anisotropic and the stability of the contacting particles decreases after releasing P_s at constant stress ratio. This evolution of the fabric anisotropy accompanying with collapse coincides with that for soils under shear. This phenomenon can further be illustrated using Figure 13. The distribution of contact normals for the specimen after P_s is deduced from 5 to 0 N (corresponding to point B in stress–strain

relationship) is quite similar to that for the specimen with constant $P_s = 5$ N at the same shear strain (corresponding to point B' in stress–strain relationship). Thus, collapse during shear may be interpreted as a shear phenomenon.

6. CONCLUDING REMARKS

In this study, a biaxial compression test on an assembly of circular rigid particles is numerically simulated using DEM by incorporating interparticle adhesive forces. The collapse behaviours of granular materials during isotropic compression and biaxial shear are simulated by releasing the interparticle adhesive forces from the initially incorporated values to zero at constant mean compression stress and constant stress ratio, respectively. The numerically simulated results are compared with the results of triaxial compression tests on unsaturated compacted clays and qualitatively similar results are obtained. The following summarizes the main collapse behaviours of granular materials obtained from the numerical simulations:

(1) The volume change induced by collapse during isotropic compression depends on the values of the initially incorporated interparticle adhesive forces and the mean compression stresses. For a specified interparticle adhesive force, the amount of the volume change is small at low and large mean compression stresses and there exists a mean compression stress where the amount of the volume change is the maximum.
(2) For a specified interparticle adhesive force, the magnitude of vertical collapsing strain ε_1 increases (compression) and the magnitude of lateral collapsing strains ε_3 decreases (extension) with an increasing stress ratio, whereas the magnitude of volumetric collapsing strain ε_v depends weakly on the stress ratio. But, the magnitude of volumetric collapsing strain ε_v may increase with an increasing interparticle adhesive force.
(3) The number of contacts at any orientation increases when collapse occurs at constant mean stress during isotropic compression and the distribution of contact normals becomes more anisotropic when collapse occurs at constant stress ratio during shear. The stability of the contacting particles decreases after collapse occurs either during isotropic compression or during shear due to the disappearance of the bonding effect of interparticle adhesive force P_s.

Finally, it is pointed out that the numerical simulation in this paper is applicable to analyse the collapse behaviours of unsaturated soils at relatively high suction where meniscuses are dominant. It appears that the method presented in the paper is still in its early development stage. In order to compare the DEM simulation results with the experimental results quantitatively, many issues remain to be addressed. They may include the development of 3D DEM simulation method or the performance of collapse tests under plain strain conditions. Nevertheless, the proposed method demonstrates its capacity in simulating qualitatively the behaviour of collapse of unsaturated soils.

REFERENCES

1. Dudley JH. Review of collapsing soils. *Journal of Soil Mechanics And Foundations Division*, ASCE 1970; **96**(3): 925–947.
2. Lobdell GT. Hydroconsolidation potential of Palouse loess. *Journal of Geotechnical Engineering Division*, ASCE 1981; **107**(6):733–742.

3. Lutenegger AJ, Saber RT. Determination of collapse potential of soils. *Geotechnical Testing Journal*, ASTM 1988; **11**(3):173–178.
4. Lawton EC, Richard J, Fragaszy RJ, Hardcastle JH. Collapse of compacted clayey sand. *Journal of Geotechnical Engineering*, ASCE 1989; **115**(9):1252–1267.
5. Lawton EC, Richard J, Fragaszy RJ, Hardcastle JH. Stress ratio effects on collapse of compacted clayey sand. *Journal of Geotechnical Engineering*, ASCE 1991; **117**(5):714–730.
6. Lawton EC, Richard J, Fragaszy RJ, Hetherington MD. Review of wetting-induced collapse in compacted soil. *Journal of Geotechnical Engineering*, ASCE 1992; **118**(9):1376–1394.
7. Pereira JHF, Fredlund DG. Volume change behavior of collapsible compacted gneiss soil. *Journal of Geotechnical and Geoenvironmental Engineering*, ASCE 2000; **126**(10):907–916.
8. Fredlund DG, Morgenstern NR. Constitutive relations for volume change in unsaturated soils. *Canadian Geotechnical Journal* 1976; **13**(3):261–276.
9. Van Genuchten MT. A closed-form equation of predicting the hydraulic conductivity of unsaturated soils. *Soil Science Society of America*, Journal 1980; **44**:892–898.
10. Alonso E, Gens A, Josa A. A constitutive model for partially saturated soils. *Geotechnique* 1990; **40**:405–430.
11. Sun DA, Matsuoka H, Yao YP, Ichihara W. An elastoplastic model for unsaturated soil in three-dimensional stresses. *Soils and Foundations* 2000; **40**(3):17–28.
12. Barden L, McGown A, Collins K. The collapse mechanism in partly saturated soil. *Engineering Geology* 1973; **7**: 49–60.
13. Mitchell JK. Fabric, structure, and property relationships. *Fundamentals of Soils Behavior*. Wiley: New York, 222–252.
14. Cundall PA, Strack ODL. A discrete numerical model for granular assemblies. *Geotechnique* 1979; **29**(1):47–65.
15. Kato S, Yamamoto S, Nonami S. Comparison of DEM simulation for biaxial compression test with results of triaxial compression test for unsaturated soil. *Journal of Applied Mechanics*, JSCE 1999; **2**:419–426 (in Japanese).
16. Ohashi T, Matsuoka H. Microscopic study on cohesion of wet aluminum rod mass. In *Proceedings of the 50th Annual Conference of JSCE*, Vol. III-164; 1995; 328–329 (in Japanese).
17. Matsuoka H. *Soil Mechanics*. Morikita Press Company: Japan; 60–63 (in Japanese).
18. Tateyama K, Fukui Y. Understanding of some behaviour of unsaturated soil by theoretical study on capillary action. In *Proceedings of Unsaturated Soils for Asia*, Rahardjo H, Toll DG, Leong EC (eds). Balkema: Rotterdam, 2000; 163–168.
19. Yamamoto S. Fundamental study on mechanical behavior of granular materials by DEM. *Doctoral Engineering Thesis*, Nagoya Institute of Technology, 1995, Japan (in Japanese).
20. Sun DA, Matsuoka H, Xu YF. Collapse of compacted clays by triaxial test. In *Proceedings of 3rd International Conference on Unsaturated Soils*, Campos T (ed). Balkema, Rotterdam 2002; 501–504.
21. Yudhbir. Collapsing behaviour of residual soils. In *Proceedings of 7th Southeast Asian Geotechnology Conference* 1982; **1**:35–53.
22. Kohgo Y, Nakano M, Miyazaki T. Theoretical aspects of constitutive modeling for unsaturated soils. *Soils and Foundations* 1993; **33**(4):49–63.